AI-based Advancements for Biomaterial Discovery: Comparative Analysis of GAN Models in Topography Generation

Karthikeyan Sivakumar
School of Computer Science
University of Nottingham
Nottingham, United Kingdom
psxks12@nottingham.ac.uk

***Abstract*—Implantable medical devices are pivotal to contemporary healthcare, yet they often induce an FBR post implantation, presenting a significant challenge. Lower attachment level biomaterials are essential in mitigating the FBR, with recent studies finding optimization methods for such surfaces. Despite these advancements, there's a shortage of samples, and crafting new topographic designs poses significant challenges and may not be feasible. This study leverages the application of Generative Adversarial Networks (GANs), including DCGANs and WGANs, to create new biomaterial topographies. The research focuses on generating complex four-by-four and simpler one-by-four topographies. Augmentation techniques are employed to enhance sample diversity, along with specially processed datasets, which yield good results. Conditional GANs are also used to create topographies based on specific biological parameters. Model efficacy is confirmed through visual and FID score analysis, revealing successful pattern learning and structural generation with notable limitations. A comparative study of GANs was conducted to identify their key insights and technological limitations. This research illustrates the capability of GANs) to synthesize biomaterial topographies, proposing innovative strategies that show promise for future research in biomaterial discovery using AI and enhancing patient care outcomes.**

***Index Terms*—Generative AI, Biomaterials, Medical Implants, GANs, Conditional GANs, DC-GANs, WGANs.**

I. INTRODUCTION

Medical implantable devices have revolutionized healthcare, enhancing patients' quality of life by combining advanced technology and human biology [1]. Since the first electrical heart stimulation in 1952 [40], this field has evolved with advancements in microelectronics, biotechnology, and materials science [38]. As Greatbatch et al. [39] outlined, today's range of implantable devices includes everything from cardiac defibrillators to cochlear implants, impacting numerous medical treatments [41].

In the United States, about one-tenth of the population, and 5-6% in other developed countries, benefit from implantable for various treatments [2][3]. However, as Wilson et al. [1], Vassey et al. [3], and Abu-Amer et al. [4] note, medical implants can pose risks, mainly due to the Foreign Body Response (FBR) post-surgery. This response can lead to complications, including allergic reactions and implant rejection [42][43]. Factors such as age, health conditions, and genetics significantly affect how a body reacts to an implant.

FBRs are macrophages, immune cells that manage foreign substances within the body and are one of the first cell types to engage with any foreign material delivered into it. The primary objective of the inflammation system is to adapt to the implant after surgery rather than FBR triggers causing damage or eliminating it. Many physical criteria influence macrophage activity, and research by Jain et al. [5] and McWhorter et al. [6] discuss the stages of inflammation and the nature of adaptation.

To avoid interacting with the implant or to control the interaction of the implant, the structure of the material plays a pivotal role [3]. The chemical composition of implant materials is vital in determining how the immune system, especially macrophages, reacts to it. Material-based strategies and initial approaches to modulate immune responses via material structure on implantation surfaces are discussed in studies by Milton et al. [7], Hucknall et al. [8], Chapman et al. [9], and Liu et al. [10]. Additionally, Veiseh et al. [11] and Vegas et al. [12] have expanded on this by exploring methods to guide the immune response through material selection and using High-Throughput Screening to identify materials optimizing immune compatibility.

Research has led to strategies for identifying materials that minimize the Foreign Body Response (FBR) and positively influence macrophage response to implants. Advanced 3D printing techniques have been pivotal in this process, allowing for the precise creation of polymers with controlled designs and material properties [3]. Chen et al. [13] and Luu et al. [14] discuss how these methods, particularly ChemoArchiChips composed of algorithmically arranged geometric shapes, can be used to study and direct macrophage behaviour in response to biomaterial topographies.

ChemoArchiChips, known as topographies, are composed of geometric primitives (circles, triangles, and rectangles) in a repetitive structure, each with specific aspect ratios and macrophage attachment levels. Research by Vassey et al. [3] indicates that topographies with lower attachment levels can substantially reduce or even eliminate the immune system's response (FBR). While current research focuses on improving biomaterials for managing attachments, there's a significant potential to expand the range of biomaterial designs, especially those featuring low macrophage attachment levels.

These new designs will be used to improve and tested in the lab before being applied to the surfaces of implants. This approach holds the potential to significantly enhance the biocompatibility and efficacy of medical implants significantly, thereby reducing the likelihood of adverse immune responses. This represents a pivotal moment at the crossroads of Artificial Intelligence and healthcare. In the evolving landscape of medical implants, the role of computer science, particularly Artificial Intelligence (AI), is becoming increasingly pivotal in advancing material design. While scientists have made progress in improving biomaterials to mitigate the FBR, the journey toward efficient biomaterial discovery remains challenging. Traditional laboratory methods for creating and testing materials are complex, time-consuming, and expensive. By harnessing the power of AI, we can significantly streamline the biomaterial discovery process, enabling the generation of diverse designs more efficiently and thereby overcoming the traditional complexities associated with biomaterial development.

Artificial Intelligence (AI) has revolutionized the computer sector, fundamentally aiming to endow machines with the capability to emulate intelligent behaviour [51]. This journey began in the early 1950s when computers were first tasked with automated intelligence functions, marking the commencement of an era where they would handle and fulfil everyday human tasks [52]. This period also saw the exploration of algorithms capable of creating synthetic data [53], laying the groundwork for future advancements in AI.

By the late 1980s, neural networks emerged as a dominant subject in both Machine Learning (ML) and AI. This era led to the invention of new methodologies and network structures [54][55], expanding the scope and capabilities of these fields. However, it was not until the late 2000s that deep learning indeed came to the forefront, sparked by pivotal research by Hinton GE et al. [56]. This publication reinvigorated neural network research after two decades of relative stagnation. Deep learning's effectiveness in capturing information and performing exceptionally in tasks like classification and regression earned it widespread acclaim. Its success in fields such as image classification and Natural Language Processing propelled it to the forefront of research. Yet, during this time, the focus was predominantly on discriminative models, while generative models received less attention, primarily due to the challenges associated with training them [57].

The transition from the early stages of AI to the advent of deep learning and beyond illustrates a remarkable journey of growth and innovation. Each phase contributed to the development of new computational models and techniques and set the stage for the next wave of breakthroughs in artificial intelligence. The evolution of AI has paved the way for ground-breaking research and applications in various fields, from its early stages in the 1950s to the emergence of deep learning in the late 2000s. The inception of Generative Adversarial Networks (GANs) by Ian J. Goodfellow et al. [58] marked a pivotal moment in generative modelling, addressing the challenges previously faced in training these models and igniting a surge of interest in their potential applications. Following the introduction of GANs, the field of generative AI experienced a renaissance, leading to the exploration and development of other innovative technologies such as VAEs and RNNs and several others. This revitalised focus on generative modelling has significantly expanded the scope and application of AI, particularly in areas that require complex data synthesis and realistic simulation.

AI has already achieved significant milestones in the medical field, demonstrating remarkable advancements in areas such as medical imaging, disease diagnosis, patient care, and more [44]. Specifically, regarding Generative AI, Ramesh et al. [46] illustrate its capabilities in creating new images and enhancing the quality and resolution of existing ones [45]. The substantial impact of AI in the medical sector paves the way for the burgeoning field of Gen AI, which promises to revolutionise healthcare and medical research [47]. Generative AI stands poised to generate synthetic data uniquely designed to meet healthcare's intricate and evolving needs, offering innovative and tailored solutions to the field's specific challenges.

In addressing the challenges of biomaterial discovery for medical implants, our approach strategically harnesses the power of generative AI, specifically emphasizing using Generative Adversarial Networks (GANs) and their variants. We have opted for GANs over other models, such as Autoencoders, VAEs, and diffusion models, due to several key factors. Firstly, GANs possess a distinctive architecture featuring a Discriminator that actively guides the generation process. This aspect is vital for creating high-quality, detailed synthetic images and crafting intricate 2D topographic objects for biomaterial research. Unlike Autoencoders and VAEs, which are primarily focused on image reconstruction, GANs offer the unique benefit of an adversarial network that excels in generating new, finely detailed content. Moreover, GANs demonstrate a superior ability to learn and adapt to the distribution of training data. This capability makes them particularly effective in generating topographies that closely

mimic real-world biological structures, aligning perfectly with our research objectives.

In contrast, diffusion models, while capable of image generation, follow a Markov chain process [86]. This process does not afford the same advantages as GANs in terms of generating detailed and diverse outputs. Additionally, diffusion models often require significant computational resources and extended processing time [87], rendering them less practical for our purposes. Considering the uncertain nature of how our data will interact with various neural network models, and after evaluating the merits and limitations of different generative models, GANs stand out as the most suitable choice. Our research employs GANs to create synthetic 2D topographic objects, aiming to delve into their capabilities for generating complex topographies. A crucial aspect of this investigation is determining whether GANs can effectively replicate the essential spatial details and complexities of these topographies, such as repetitive structures and spatial configurations, key requirements for advancing biomaterial research.

Furthermore, our methodology involves a unique interplay between Computer Science and biomedical engineering, where we integrate biological information into the GANs as a form of conditioning. This approach leads us to delve into the application of conditional GANs, examining their effectiveness in producing images that correspond with specific labels, mainly focusing on the attachment levels of the topographies. Such integration is pivotal for creating tailor-made topographies that align with specific biological requirements. Crucially, this exploration establishes the feasibility of using CGANs to generate images related to and accurately represent the labelled attachment levels of these topographies.

This symbiosis of AI technology with biological insights is expected to yield significant advancements in the design and functionality of medical implants, paving the way for more personalised and effective biomaterial solutions. Controlling Foreign Body Response (FBR) in medical implants is paramount to enhance patient outcomes, safety, and quality of life. FBR can influence the effectiveness and longevity of implants, making it a critical area of study in healthcare and biomaterials research. Central to this study is the investigation into how GANs focus on the shapes of the topographies, particularly examining the proficiency of GANs in emphasising the pre-processed images crucial in directing the network's attention to specific topography shapes. This aspect of the research aims to determine the effectiveness of GANs in accurately capturing and emphasising the vital characteristics of the topographies, a factor essential for the advancement of biomaterial design.

The future of biomaterials and medical implants will rely on integrating advanced AI applications and novel computational techniques [59]. The utilisation of Generative AI models like GANs, in particular, offers the potential for accelerating the discovery process. AI's proficiency in pattern identification is crucial for comprehending complex datasets, enhancing our understanding of current research data and paving the way for deeper insights and further advancements in the field with targeted research efforts. A pivotal element of our research involves comprehensively comparing various Conditional GANs and GAN models, evaluating how each distinctively generates images. This examination is critical to understanding their applicability and effectiveness in biomaterial research. Moreover, assessing the quality of the images produced by these models is crucial, as it is a vital metric in determining their practical utility for medical implant design. By contrasting different GAN architectures, the research aims to offer a detailed analysis of their capabilities and limitations, thereby making a substantial contribution to AI-driven biomaterial innovation.

By analysing health data, AI can design biomaterials that specifically address a patient's unique medical conditions, offering a level of personalisation previously unattainable with conventional methods. In line with these advancements, our research will further investigate critical technical aspects to enhance AI's efficacy in biomaterial design. We aim to determine if increasing the sample size of the topographies through rotation can improve the model's performance. Additionally, a crucial part of our investigation is to ascertain whether two by two cropped topographies retain essential information about the spaces between the topographies, a vital factor for ensuring the versatility of our biomaterial designs and evaluating the performance of GANs in scenarios where redundant data is minimised. Thus, by embracing these opportunities and addressing these specific research questions, medical implants can move towards more efficient and innovative solutions, ultimately improving patient care and treatment outcomes from synthetic data [60].

II. LITERATURE REVIEW

In the rapidly evolving domain of biomaterials research, a detailed exploration of the literature unveils an intricate understanding of the field's dynamic capabilities and complexities. Numerous studies have skilfully highlighted the challenges in biomaterial discovery, emphasizing the current and anticipated obstacles. A consistent theme in this body of work is the acknowledgment of the critical need for further innovation in biomaterials, pointing towards a promising and transformative future for the field.

A significant and emerging aspect of recent research is the proposal to incorporate artificial intelligence (AI) to augment biomaterial research. While initial steps have been taken in this direction, the full potential of AI in driving biomaterial discovery remains largely untapped. This gap presents an exceptional opportunity to merge computer science and biomaterials, potentially revolutionizing how we approach

innovation in this field. Specifically, the application of AI in addressing complex challenges in medical implant design and fabrication is an area ripe for exploration.

The study by Prakash et al. [79] provides a comprehensive review of advancements in deriving mesenchymal stem cells (MSCs) from pluripotent stem cells (PSCs), with a focus on biomaterial-based methodologies. The authors discuss the pros and cons of sourcing MSCs from adult and infant tissues, underscoring the need for more uniform and proliferative sources. They also explore the potential of PSCs, like embryonic stem cells and induced pluripotent stem cells (iPSCs), to differentiate into various cell types, including MSCs. This review compares traditional MSC sources and cutting-edge techniques for deriving MSCs from iPSCs, emphasizing the significant role of biomaterials in two-dimensional and three-dimensional culture systems. The study concludes by positioning PSCs as a promising alternative for MSC production, highlighting the opportunities to develop more efficient methods for their clinical application.

Hendrikse et al.'s [80] review delve into the design of synthetic biomaterials, focusing on the crucial roles of molecular organization, chirality, and spatial configuration. These elements mirror the complexity of fundamental biological building blocks, such as nucleotides, amino acids, and saccharides. The review confronts the challenges of replicating these intricate natural structures in synthetic materials and stresses the importance of incorporating order and handedness for successful biological interactions. It evaluates both natural and artificial systems, spotlighting the role of computational simulations in enhancing design. The review concludes by emphasizing the necessity of hierarchical organization and complexity in biomaterials for improved biomedical applications, advocating for integrating these elements in future biomaterial development.

Kajal Babani et al.'s [81] paper reviews the evolution of biomaterials, particularly in their integration with tissue engineering and 3D printing for medical applications. It traces the journey from initial biocompatibility discoveries to utilizing various materials like metals and polymers in medical implants. The paper highlights the pivotal role of 3D printing in creating biocompatible structures for tissue regeneration and discusses the advancements in 3D-printed organs, such as skin and hearts. It also addresses the challenges in 3D printing and its potential to provide personalized medical treatments, thereby reducing the reliance on organ donors and addressing transplant rejection issues. The paper concludes that the convergence of biomaterials, tissue engineering, and 3D printing represents a significant advancement in healthcare, enhancing treatment methods and overall quality of life.

A. I. Pais et al.'s [82] paper examines the development and application of cellular materials in biomechanics, focusing on tissue engineering and implant design. The paper underscores the significance of the porous structure of these materials in promoting bone growth. It also details how computational methods like AI, machine learning, deep learning, and multiscale modelling enhance these materials' mechanical properties and design. Covering aspects from biocompatibility to porosity management, the authors present a comprehensive view of current trends and prospects in orthopaedic biomechanics, highlighting the growing importance of computational techniques in this evolving field.

The study by Benita et al. [83] explores the potential of artificial intelligence (AI) in advancing regenerative medicine, particularly in bone regeneration through tissue engineering. The paper underscores AI's capability to tackle key challenges in the field, such as optimizing biomaterial designs and enhancing stem cell research. The methodology focuses on AI's application in analysing complex data, selecting appropriate deep learning architectures like CNNs and GANs, and finetuning hyperparameters for effective training while addressing overfitting and data bias. The research proposes evaluating AI models based on their impact in reducing time and resources in tissue engineering and enhancing scientific understanding. The paper highlights AI's role in developing patient-specific and trauma-specific solutions in bone regeneration and tissue engineering.

Rachel K's [84] research presents developing and applying a specialized large language model (LLM) named BioinspiredLLM, built on the Llama-2-13b-chat framework. This model excels in accurately recalling information, generating hypotheses for unexplored research areas, and aiding in task creation and prompt engineering tasks. BioinspiredLLM's unique capabilities include generating creative insights and hypotheses about biological materials, even those not explicitly covered in its training data. The model's evaluation focused on its knowledge recall accuracy, creativity in hypothesis generation, conversational coherence, and utility in research tasks, achieving a 98% accuracy rate in repeated trials. The model enhances bio-inspired materials research by synergizing with AI tools, with future improvements aimed at dataset expansion and broader scientific integration, highlighting the need for careful verification.

Yu-Hsuan Chiang et al.'s [85] study focuses on developing a deep generative network, specifically an AE-TransformerGAN (AutoEncoder-Transformer Generative Adversarial Network), to efficiently generate 3D bioinspired microstructures. This model integrates the Transformer network architecture, known for its proficiency in handling sequential data, into a GAN framework, adept at creating 3D models from limited training data. The methodology involves using the AETransformer-GAN to learn from a limited set of microstructures, such as periodic gyroids and complex elk antler structures, and generate numerous 3D samples with analogous structural features. The evaluation includes

comparing generated structures with original microstructures using various analytical methods, such as porosity profile analysis, pore size distribution, and the Image-Based Invasion Percolation (IBIP) algorithm. The research holds promise for various engineering applications, suggesting a new frontier in replicating and understanding complex biological and bioinspired materials.

Finally, the applications of GANs, as illustrated in studies by Osokin et al. and Baniukiewicz et al., hint at the possibility of leveraging GANs in biomaterial research. However, direct applications in this specific field are not extensively documented. Similarly, while studies by Menon et al. [18] and Coto, Andrea et al. [50] demonstrate the impressive capabilities of GANs in materials science, the translation of these methodologies to the specific requirements of biomaterial discovery for medical implants has yet to be thoroughly pursued. In parallel, insights from surveys by Arora et al. [48] and research by Skandarani Y et al. [49] in medical imaging, though not directly related to biomaterials, shed light on the potential of GANs in processing complex medical data. This skill is highly relevant and applicable to biomaterial discovery. Furthermore, the application of GANs in drug discovery, as explored by Blanchard et al. [16], indicates the potential of these networks in identifying and creating novel materials. This concept could be extended to biomaterial discovery.

Recent studies in biomaterials research, such as those by Prakash et al. [79] and Hendrikse et al. [80], underscore a growing focus on tackling the inherent complexities in biomaterial development. These works highlight the need for advanced methodologies in synthetic biomaterial creation, pointing towards a trend of more intensive research in this area.

Similarly, Kajal Babani et al. [81], A. I. Pais et al. [82], and Benita et al. [83] emphasize the integration of advanced computational technologies and AI to enhance biomaterials' utility and confront medical challenges. Remarkably, the potential of AI in biomaterial discovery, as discussed in [83], aligns with our research in discovering topographic primitives. Studies [84] and [85] further illustrate AI's relevance in biomaterials, serving as an inspiration for leveraging AI as a transformative tool in our biomaterial innovation research.

Our comprehensive review in the biomaterial domain has unearthed several pivotal insights. Most notably, there is a discernible scarcity of research directly employing artificial intelligence (AI) in biomaterial discovery. Although AI has found applications in various aspects of biomaterial research, it is increasingly evident that this domain is ripe for more extensive exploration. The current landscape in biomaterial research, gradually integrating AI, points to a significant gap in specialized research. This gap underscores an unmet need and opens avenues for ground-breaking research opportunities in this field. This observation highlights the critical need for more focused and profound research endeavours in AI's application to biomaterial discovery. It presents a unique and timely opportunity to pioneer innovative research paths that could substantially contribute to reshaping the biomaterials for medical implants landscape using AI.

This research aims to address this gap by applying GANs to the design of biomaterials for medical implants, thereby making a substantial contribution to the advancement of AI technology and biomedical engineering. While Generative Adversarial Networks (GANs) have seen significant success in various domains, particularly in biology and materials research, their direct application to biomaterial research for medical implants remains underexplored. Although the broader field of Generative AI has transformed numerous industries with the production of synthetic yet realistic data, its potential in surface topology optimization is yet to be fully realized. Despite the broad applications of GANs as demonstrated in these studies, the literature explicitly focusing on their application in biomaterials for medical implants is still being determined, and this research will leverage GANs and GAN variants for 2D topographic discovery.

Positioned at the convergence of these two fields, our investigation seeks to push the boundaries of biomaterial innovation using computer science. It represents a pioneering effort to explore how AI can be leveraged to revolutionize biomaterial development. It marks a significant step forward in charting a new interdisciplinary research and application direction.

III. INTRODUCTION TO DATASET

For our research, the Bio-Material Dataset primarily comprises grayscale images of various bio-material samples. A dataset consisting of 2176 topographic images was given, and a four-by-four ratio followed the patterns. A machine learning approach was used to generate the 2D topographic images, and an example of the image is attached below in Fig 1. Complementing this dataset, we had access to additional data on macrophage attachment levels, provided for 2100 images. This data, categorized into five unique values, was stored separately in a CSV format, integrating an essential dimension to our analysis. In further analysis, we encountered that the dimensions of the dataset range from 300X300 to 1220X1220.

Before deciding, it's good to understand the dataset's unique intricacies and structure, which is crucial for navigating the complexity inherent in the research. Likewise, in this research, we encountered several challenges that directly reflect the current limitations of technology. A primary challenge was the limited number of samples available. Each sample possesses unique and significant attributes, making standard oversampling techniques commonly used in data pre-processing for neural networks inappropriate. Utilizing such

techniques could result in the loss of critical information about the topographies' attachment level, an essential aspect of our study.

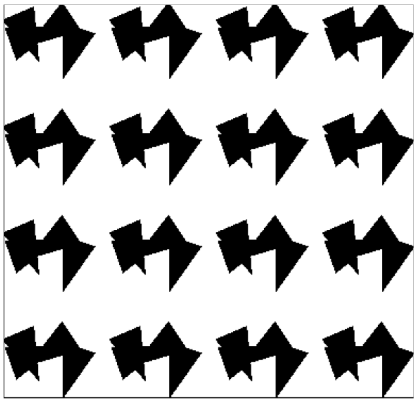

Fig. 1. Example of 2D Topographic Image

Another significant challenge was managing the varying dimensional ranges of the images in the dataset. Coupled with this was the task of determining the optimal pixel size for image generation. High cardinality in pixel size necessitated a careful balance between maintaining image quality and computational feasibility. Selecting a large pixel size could escalate computational costs, thereby limiting our ability to deepen the neural network or further tune the model for optimization. This study established unique strategies to efficiently handle the challenges that were addressed in pre-processing, ensuring the integrity of our approach to research while resolving the inherent intricacies of the data.

IV. METHODOLOGY

A. Pre-processing the Dataset

Upon analysing the dataset, it became apparent that the topographies had varying dimensions, with over 90 unique height and width combinations. To prepare the images before feeding into the neural network input, a decision was made to resize all images to a consistent dimension of 256x256 pixels. However, resizing presented a challenge, often resulting in losing image quality.

- Interpolation Method: An interpolation method will be employed to mitigate the loss of image quality during resizing [20]. While interpolation does introduce some level of pixel degradation, it helps preserve image quality to a considerable extent.
- Cropping Strategy: Another approach was to utilize the repetitive nature of topographies. An interesting observation was made by cropping the images to focus on their initial sections, as mentioned in Figure 2.

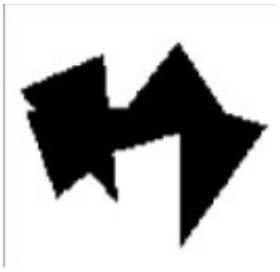

Fig. 2. Example of Cropped topology from 4-by-4 figure.

After cropping the dataset, we encountered another obstacle to holding the spatial information and reducing the computational expense. To preserve the space of the topographies, another approach was made to retain the attachment information, as mentioned in Figure 3.

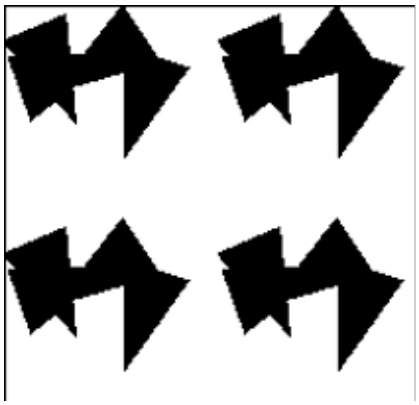

Fig. 3. Example of 2 by 2 Cropped Topography.

Instead of cropping the image into initial sections, which are one by one, the topographies are cropped into two by two, thus preserving the distance between the biomaterials and reducing the computational load. Once the images are generated from two-by-two topographies, reverse engineering can be done, or the images can be mapped to four-by-four to get the default structure of the materials.

Since Generative Adversarial Networks (GANs) require a substantial amount of training data for effective performance [21], a strategic decision will be made considering the limited availability of training data in this case. Data augmentation is a technique used to enhance the size and quality of training datasets such that better model performance can be achieved and overfitting can be mitigated [22]. By applying transformations such as image rotation, the original dataset comprising 2176 images can be expanded to 8704 images, thereby enriching the diversity of the training data. Examples of these rotations are illustrated in Figure 4.

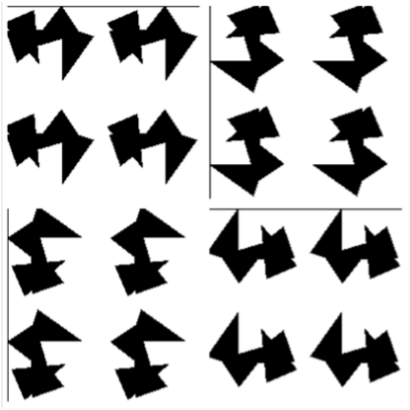

Fig. 4. Example of 2 by 2 Rotated Topography.

After examining the image variants, we observed that the pixel distribution of the cropped images revealed three distinct segments, as illustrated in the pie chart in Figure 4.

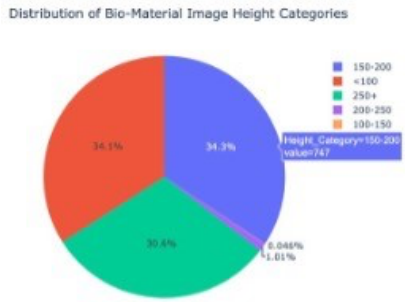

Fig. 5. Pixel distribution of Cropped Image

To ensure consistency across the dataset, the 1/4 images with dimensions smaller than 100 pixels will undergo an upscaling process. Conversely, images exceeding 192 pixels in size will be subjected to downscaling using interpolation. The chosen pixel size for standardization, 192 pixels, is derived from the average dimensions of the cropped images within the dataset. This upscaling approach aims to balance preserving image quality, retaining critical information, and improving the model's efficiency by preventing quality degradation due to a loss of detailed information [23].

In the case of upscaling, two specialized architectures, EDSR (Enhanced Deep Residual Networks for Single Image Super-Resolution) and LapSRN (Laplacian Pyramid Super-Resolution Network) models, were employed [24][25]. These deep learning models are designed specifically for image super-resolution (SR) tasks and outperform traditional methods [26], such as Nearest Neighbor Interpolation [27] and Bilinear Interpolation [28], among others.

- **Upscaling using Super Resolutions:**

a. ***Enhanced Deep Residual Networks for Single ImageSuper-Resolution:***

EDSR, a pivotal development in the field of super resolution, is an innovative amalgamation of the Deep Residual Network (ResNet) concept [32] and the Super Resolution models [33][37]. Super-resolution models are fundamentally designed to reconstruct high-resolution images from their low-resolution counterparts. They play a crucial role in enhancing image quality, particularly in scenarios where high-resolution data is not available and hard to obtain [36].

The foundational principle of a Residual Network lies in its residual blocks, which consist of convolutional layers followed by normalization and activation functions. These blocks enable effective learning through skip connections or shortcut connections. These skip connections are instrumental in mitigating the vanishing gradient problem, facilitating the training of deeper networks by allowing the gradient to flow directly through the network [35].

In the realm of super-resolution, the authors [34] et al. adapted the ResNet architecture, leading to the inception of the Super Resolution ResNet (SRResNet). This adaptation laid the groundwork for EDSR, and the framework builds upon SRResNet by analysing and removing modules deemed unnecessary for super-resolution tasks. This simplification of the network architecture, coupled with targeted modifications, significantly enhances performance, making EDSR a powerful tool in the field of image super-resolution.

b. ***Laplacian Pyramid Super-Resolution Network:***

On the other hand, LapSRN has a unique way of upscaling the image among super-resolution models, and it's well known for its fast and accurate results. It is a significant advancement in the domain of super-resolution and represents an ingenious integration of the Laplacian pyramid concept with state-of-theart deep learning techniques.

The core innovation of LapSRN lies in its unique utilization of the Laplacian pyramid structure, a method traditionally used in image processing for representing an image at multiple scales. This multi-scale approach is adeptly adapted into a deep learning framework, enabling the progressive reconstruction of images from low to high resolution [25]. Each level of the Laplacian pyramid in LapSRN corresponds to a different resolution scale, ensuring a meticulous and incremental enhancement of image detail.

Unlike traditional super-resolution models that attempt to upscale images in a single, often complex leap, LapSRN introduces a cascading architecture where each stage focuses on upscaling the image to a slightly higher resolution. At the heart of LapSRN are deep convolutional neural networks (CNNs) that operate at each level of the pyramid. This gradual upscaling process mitigates the risks of losing important

features in the image and improves the quality of the upscaled images [61].

- **Applying Gradient filter and transforming:** To ensure that the model focuses more on emphasizing the shapes of the topographies, this paper will utilize a novel traditional method known as the morphological gradient [20]. The morphological gradient is the difference between an image's dilation and erosion. It highlights the edges or boundaries of objects within the image. This gradient was applied to the 1/4 cropped topography datasets, and the example is shown in Figure 6 below.

Fig. 6. Example of a Gradient transformed topography.

B. Model Selection

Having established a deep understanding of the dataset and the necessary pre-processing steps, we now transition to the core of our methodology, where we focus on selecting and applying various Generative Adversarial Network (GAN) models. Our strategy involves a comprehensive comparative analysis of several GAN architectures, each chosen for its unique attributes and potential efficacy in synthesizing synthetic biomaterial topographies. In this section, we will examine a range of GAN models, including Vanilla GANs, Conditional GANs (C-GANs), Deep Convolutional GANs (DC-GANs) and Wasserstein GANs (W-GAN).

Each model's architecture is described, highlighting how their specific design and features are tailored to meet the intricate requirements of generating topographical images for biomaterials. We delve deeply into each GAN variant's distinct characteristics and operational mechanisms, emphasizing how they respond and adapt to our specialized dataset. This detailed examination will underscore each GAN variant's distinctive capabilities and provide insights into their applicability and effectiveness in the context of biomaterial discovery research. Finally, our analysis will be pivotal in understanding how these models can be leveraged to simulate complex spatial characteristics and meet the intricate requirements of generating topographical images for biomaterial applications.

The architecture of Generative Adversarial Networks (GANs) fundamentally hinges on the dynamic between two critical neural networks: the Generator (G) and the Discriminator (D). The Generator, denoted as G(z), is tasked with producing synthetic data from a random noise input z by taking a vector of random noise as input and transforming this noise into data that resembles the target distribution. Conversely, the Discriminator, represented as D(x), evaluates the data x, discerning actual data from the dataset against the fake data generated by G, as illustrated in Figure 7.

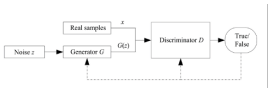

Fig. 7. Illustrates the working of GANs.

The core objective of GANs is encapsulated in the following equation:

$$\min G \max DV(D, G) = Ex{\sim}pdata(x)[\log D(x)] + Ez{\sim}pz(z)[\log(1-D(G(z)))]$$

In this formulation, $E_{x\sim p\text{data}(x)}[\log D(x)]$ signifies the Discriminator's proficiency in correctly identifying real data. The term $E_{z\sim pz(z)}[\log(1 - D(G(z)))]$ represents the Discriminator's ability to detect fake data generated by the Generator. The Generator aims to minimize this function to produce data indistinguishable from real data, while the Discriminator endeavours to maximize it, accurately classifying real and generated data.

The Generator and Discriminator in this adversarial setup are typically designed as deep neural networks. These networks may consist of multiple layers, depending on the complexity required for the task. The layers effectively capture spatial hierarchies in the data with the training process involving key parameters like epochs, batch size, normalization, and z-dimension values. Epochs determine the number of complete passes through the dataset during training, balancing the learning without underfitting or overfitting [88]. Batch size, the number of samples processed in one iteration, affects learning dynamics and computational efficiency. Normalization, like batch normalization, stabilizes the training by normalizing inputs within each mini batch. The z-dimension value defines the noise vector's size, influencing the generated data's variety and complexity.

The training of GANs involves a delicate balance achieved through the iterative backpropagation process. This process consists of optimizing the network weights, where the role of optimizers becomes crucial [89]. Optimizers, such as Adam or Stochastic Gradient Descent (SGD), are algorithms that adjust the weights to minimize the loss function. The loss function quantifies the difference between the predicted and actual outputs [90], guiding the Generator in producing more realistic data while aiding the Discriminator in improving its detection accuracy.

Activation functions also play a vital role in GAN architecture. These functions, such as ReLU (Rectified Linear Unit) or Tanh,

are applied to the output of each neuron and determine whether it should be activated. They introduce non-linearity to the network, allowing it to learn complex patterns. In GANs, activation functions like Leaky ReLU in the Discriminator help prevent the vanishing gradient problem, which is crucial for maintaining model robustness [58]. The Generator often uses Tanh or similar functions in its output layer to ensure the generated data aligns with the actual data distribution.

Thus, the interplay of the architecture, optimizer, loss function, and activation functions facilitate the continuous refinement of both networks in GANs. The Generator progressively enhances its capacity to craft realistic data while the Discriminator advances in distinguishing accurate data from synthetic. This synergy empowers GANs to generate high fidelity synthetic data, a capability that proves invaluable in domains demanding precise and detailed data generation, such as biomaterials research.

- **Vanilla GANs:**

In our study, the Vanilla Generative Adversarial Networks (GANs) are the foundational model due to their straightforward yet effective architecture. A Vanilla GAN consists of two pivotal components: the Generator (G) and the Discriminator (D). Both these components are implemented using Multilayer Perceptron (MLPs), renowned for their ability to recognize and learn patterns [61]. An MLP, a classic feedforward artificial neural network, comprises three layers: an input layer, several hidden layers, and an output layer. Each neuron in one layer connects with every neuron in the subsequent layer. Through the training process, these weights are fine-tuned to optimize performance.

Initially, our approach involved a standard two-layer MLP for the Generator and the Discriminator, with the Adam optimizer for network training. This setup provided a baseline for generating synthetic data and assessing the model's initial effectiveness. As we progressed, the complex nature of biomaterial topographies necessitated a tailored approach. We shifted to a more advanced custom implementation, experimenting with different layer configurations and the number of neurons and tuning the other parameters to refine the model's generative capabilities.

A significant enhancement in our custom implementation of Vanilla GANs was the inclusion of dropout layers, particularly in the Discriminator. Dropout layers are a form of regularization technique used to prevent overfitting in neural networks and are addressed by randomly turning off a subset of neurons during the training phase [62]. This ensures that the model does not over-rely on specific training data features and provides a balanced learning process [63] in the context of GANs, where an overpowering Discriminator can stifle the Generator's learning ability [64]. By implementing dropout layers, we preserved the delicate equilibrium essential for the adversarial training process, thus enhancing the model's ability to generalize and fostering a competitive yet fair environment for both networks to improve.

- **C-GANs:**

In transitioning to Conditional Generative Adversarial Networks (C-GANs), we embraced a more targeted approach to generating synthetic data. C-GANs diverge from Vanilla GANs by incorporating an additional condition or label input, which serves as a directional guide for the data generation process. This conditional label is integrated into the Generator and the Discriminator, enabling the model to tailor the data generation to the given condition [65].

In our research, the feature of C-GANs was leveraged to create images that correspond to specific macrophage attachment levels, crucial for our study of Biomaterial Discovery. In the architecture of C-GANs, the condition is typically concatenated with the input layer of both the Generator and the Discriminator. Such integration allows the Generator to produce data that not only mimics the distribution of the training set but also aligns with the specified conditional inputs. The Discriminator, now evaluating data based on authenticity and condition compliance, becomes more precise in its classifications.

Our initial approach with C-GANs began with a standard four-layer MLP model, adhering to established practices in the field. As we delved deeper into the nuances of biomaterial topography, our methodology evolved, incorporating over thirty different architectural combinations. This iterative process included integrating batch normalization to improve network stability, employing dropout layers to prevent overfitting, and exploring a blend of these techniques. Moreover, we experimented with alternative loss functions like Mean Squared Error and Wasserstein loss to fine-tune the model's performance. The structure of both the Generator and Discriminator was meticulously adjusted, with layer counts varying up to eight layers, to optimize the generative process. Each methodological adjustment was driven by the goal of refining the model's sample generation capabilities, which could be pivotal in advancing biomaterial discovery.

- **DC-GANs:**

As our research progressed, it became evident that the Vanilla GANs were approaching a saturation point, particularly in their capacity for pattern recognition. The inherent structure of Vanilla GANs, based on Multilayer Perceptron's (MLPs), posed computational challenges [66], especially when handling gradient-filtered image datasets. The computational expense of MLPs and their limited effectiveness in discerning intricate patterns [66] led us to explore alternative architectures. These considerations led us to adopt Deep Convolutional Generative Adversarial Networks (DC-GANs). DC-GANs, with their convolutional layers, offered a significant advantage in processing 2D spatial data [67], thus presenting a more suitable solution for our biomaterial topography generation. The shift

to DC-GANs marked a strategic pivot in our approach, aligning with our goal to enhance the model's performance in generating high-resolution, accurate topographic images.

The defining feature of DC-GANs lies in their unique architecture, which eschews fully connected layers in favour of convolutional layers for deeper network segments. This design choice enables the network to grasp spatial correlations more adeptly within the data [67], facilitating the generation of high-resolution images. The Generator's convolutional-transpose layers skilfully magnified the input noise into detailed synthetic images. In contrast, the Discriminator's convolutional layers became adept at feature extraction and analysis, greatly enhancing the fidelity of pattern recognition [68].

A cornerstone of our DC-GANs research was incorporating residual blocks within the network architecture. These blocks consist of sequences of convolutional layers, batch normalization, and activation functions, creating shortcuts that allow layers to learn residual functions relative to the layer inputs. This setup facilitates the uninterrupted gradient flow, allowing deeper network constructions without succumbing to the vanishing gradient problem [35]. Including residual blocks was strategic, enabling the network to learn more complex mappings and achieve stability across extensive training epochs.

Our methodology thoroughly explored hyperparameters and structural nuances within the DC-GAN framework. We tailored the number of convolutional layers, experimented with various filter sizes, and fine-tuned the kernel sizes and stride lengths. This level of customization was pivotal in refining the model's ability to generate synthetic biomaterial topographies that not only mirrored the complexity of the input data but also expanded the potential for new pattern discovery. The transition to DC-GANs was a calculated strategy informed by the specific challenges of biomaterial synthesis. It aligned our computational resources with our ambitious research goals, enabling us to push the boundaries of what's possible in synthetic image generation for biomaterials.

- **W-GANs:**

Our pursuit of precision in biomaterial topography generation led us to a critical juncture where the conventional GAN models, particularly DC-GANs, began to show limitations. The challenges were most pronounced when generating structures with repetitive elements, such as 2x2 and 4x4 patterns. We observed inconsistencies and a lack of uniformity in the synthetic images produced by DC-GANs, which propelled us to explore more advanced GAN architectures.

Introducing Wasserstein GANs (WGAN) and their advanced variant, WGAN with Gradient Penalty (WGAN-GP), marked a significant evolution in our methodology. These models were specifically chosen for their innovative loss calculation approach and inherent stability during training. WGAN introduces the Wasserstein loss, which computes the Earth Mover's distance, providing a more robust gradient for the Generator [69]. This was a pivotal shift from traditional GANs, where vanishing gradients often led to unstable training and mode collapse – a recurring challenge with our DC-GAN experiments. WGAN-GP further advances this concept by incorporating a Gradient Penalty into the loss function. This addition mitigates the challenges posed by weight clipping in standard WGANs, ensuring consistent gradient behaviour throughout the training process [70]. This stability is crucial in maintaining a balanced dynamic between the Discriminator and Generator, addressing an imbalance we frequently encounter in DC-GAN models.

Our strategic shift to WGAN was driven by the need to overcome specific challenges in generating complex biomaterial topographic studies. These models are proven to improve stability and reduce the risk of mode collapse more than any other Gan variants [71], which is required for matching the intricate details and consistent patterns in our biomaterial discovery journey. Through WGAN, we have moved closer to achieving our overarching goal of synthesizing biomaterial designs with high fidelity and precision.

V. EVALUATION

Before delving into the detailed evaluation of the various Generative Adversarial Network (GAN) models employed in our study, it is essential to establish the framework and criteria for this assessment. The evaluation of GAN models in the context of biomaterial topography generation is multifaceted, incorporating both qualitative and quantitative analyses.

Our primary objective is to gauge the efficacy of each model in producing high-fidelity synthetic images that accurately replicate the intricate patterns and structures of biomaterial surfaces. To this end, we employ a combination of visual inspection and Frechet Inception Distance (FID) scores [91].´ Visual inspection allows us to qualitatively assess the aesthetic and structural integrity of the generated images. At the same time, FID scores provide a quantitative measure of the similarity between the distributions of generated and real images.

Each GAN variant generated a set of 16 images for a comprehensive and balanced evaluation. The FID scores were then calculated for these batches to assess the consistency and quality of the generated images across different model configurations. This methodology ensures uniformity in evaluation and allows for a fair comparison of the various GAN variants. This comprehensive approach enables us to critically compare the performance of each GAN variant, from Vanilla GANs to the more advanced WGAN models, thereby identifying the most effective techniques for biomaterial topography synthesis in our research.

A. Vanilla GANs

In our initial exploration of Vanilla Generative Adversarial Networks (GANs), we gleaned fundamental insights into the capabilities and limitations of generative modelling for biomaterial topography synthesis. Our evaluation focused on two specific topographical patterns: 1 by 4 and 4 by 4, utilizing different datasets. The foundational architecture, derived from existing literature, served as an essential starting point, though the results while capturing some patterns, indicated room for improvement and guided our progression towards a custom architecture.

In our customized approach, we experimented with over six combinations, generating images and calculating their corresponding Fréchet Inception Distance (FID) scores, shown´ in Table I.

For the one-by-four topography, using a standard dataset of 2176 images, our three combinations yielded promising results with closely competitive scores. A Vanilla GAN generated the most successful batch with a 4-layer architecture for the Generator and Discriminator, incorporating dropout layers in the Discriminator and a learning rate of 0.0002. This configuration achieved an impressive FID score of 419.2180318452365 and the generated image is shown in Figure 8.

TABLE I

ILLUSTRATES THE FID SCORES OF THE VANILLA GAN COMBINATIONS.

Vanilla GAN Combination Names	FID Score
4 by 4 Vanilla GANs 4 Layer - Eps = 200	496.7845755492306
4 by 4 Vanilla GANs 4 Layer - Eps = 250	497.99034096661757
4 by 4 Vanilla GANs 4 Layer - lr = 0.0002 - 200 Eps	488.18345876536063
1 by 4 - Vanilla GANs - 4Layers - 200eps	422.98492524014284
1 by 4 - Vanilla GANs- 64X64 - 200 Eps - lr = 0.0002	419.21803184852365
1 by 4 - Vanilla GANs- 64X64 - 200 Eps - lr = 0.0003	427.8725253176444

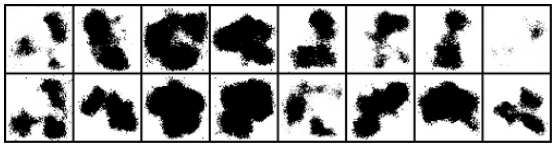

Fig. 8. Illustrates the one-by-four GAN generated image.

Similarly, all three combinations produced satisfactory results for the four-by-four topography. The top-performing batch in this category was also generated by a Vanilla GAN with a 4-layer architecture, dropout layers in the Discriminator, and a learning rate of 0.0002, resulting in an FID score of 488.18345876653063 and the generated image is shown in Figure 9.

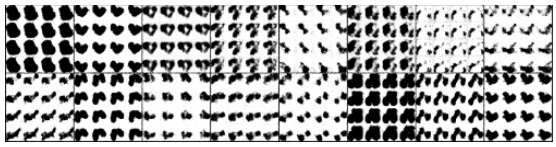

Fig. 9. Illustrates the four-by-four GAN generated image.

In testing Vanilla GANs with larger sample sizes, we evaluated models for two-by-two and four-by-four topographies using resized and rotated datasets. Notably, the models demonstrated improved performance, with the two-by topography model scoring an FID of 478.16585930439976 and the four-by-four topography model excelling with an FID of 448.3321029119707.

However, the exploration with gradient filter-applied datasets revealed a significant limitation. The MLP-based Vanilla GANs struggled to process these datasets, underscoring the model's constraints in handling more complex data transformations. These findings from our Vanilla GAN evaluation shed light on the model's potential and boundaries in biomaterial discovery and paved the way for exploring more advanced GAN architectures.

B. Conditional GANs

The progression of our research into Conditional Generative Adversarial Networks (C-GANs) marked a significant shift toward more specialized and targeted generative modelling. C-GANs, with their unique ability to incorporate conditional inputs, allowed us to generate biomaterial topographies that were aligned with specific parameters, such as macrophage attachment levels. This section presents the results of our CGAN experiments, highlighting their effectiveness in creating detailed and condition-specific topographies.

To comprehensively evaluate the performance of C-GANs, we conducted a series of experiments with 25+ different architectural configurations and combinations, and all the next combinations were pursued after reaching their saturation point. The results of each of the combinations are shown in their respective places. Our exploration of Conditional Generative Adversarial Networks (C-GANs) focused on their ability to generate biomaterial topographies, precisely the 4x4 pattern, conditioned by a dataset of 2100 topographies. This choice was strategic and aimed at testing the models' capacity to capture spatial details, replicate repetitive structures, and adhere to specific attachment level conditions.

- **4 Layer C-GAN Architecture:**

Our exploration spanned four distinct combinations in the realm of 4-layer C-GAN Architecture. Each model demonstrated commendable performance during visual inspections, a vital step preceding our FID evaluations. As presented in the accompanying Table II, the results reveal a

relatively narrow FID score range across these models, with a maximum variance of approximately 40 points.

TABLE II

ILLUSTRATES THE FID SCORE FOR 4 LAYER C-GANS

C-GAN Combination Names	FID Score
C-GAN using ANN 4 Layer G & D BCE Loss EPS = 200	474.7411320123402
C-GAN using ANN 4 Layer G & D BCE Loss EPS = 250	509.0256116218969
C-GAN using ANN 4 Layer G & D BCE Loss Eps = 200 dim = 112	502.98547592438734
C-GAN using 4 Layer G & D - BCE Loss - eps = 250 Z dim = 112	507.7035363649482

Notably, the standout model within this group was the 4 Layer C-GAN, equipped with both Generator and Discriminator and utilizing BCE Loss throughout 250 epochs. This configuration achieved an impressive FID score of 474.7411320123402, marking it the most effective in generating bio-material topographies, as shown in Figure 10.

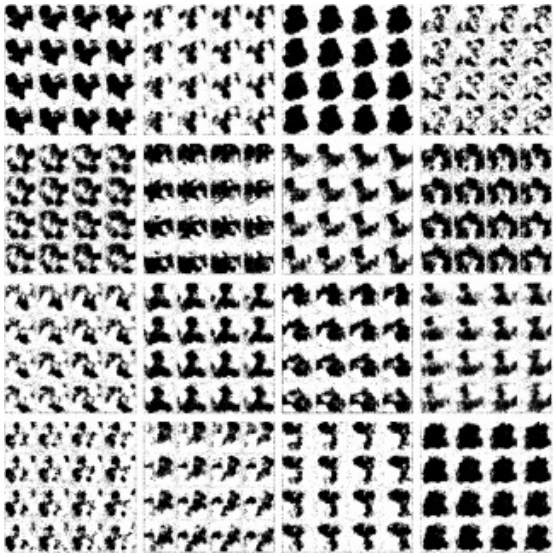

Fig. 10. Illustrates the C-GAN generated Image on 4-Layer Architecture.

- **5 Layer C-GAN Architecture with BCE LOSS:**

Expanding to a 5-layer C-GAN setup with BCE Loss, we investigated six combinations, including one with BCEwithLogitLoss. Through visual assessments and FID evaluations (see Table III), we found the C-GAN with a 5 Layer Generator and Discriminator, 200 epochs, and a z-dimension of 112 to be the most effective, achieving an FID score of 499.2763402028513 is shown in Figure 11.

TABLE III

ILLUSTRATES THE FID SCORE FOR 5 LAYER C-GANS WITH BCE LOSS

C-GAN Combination Names	FID Score
C-GAN using ANN 5 Layer G & D BCELoss - Eps = 200 - z dim = 112 TUNING	509.50546782739595
C-GAN using ANN 5 Layer G & D BCELoss Eps = 250 - z dim = 112	512.1563970357131
C-GAN using ANN 5 Layer G with Batch Norm of 3Layers BCELoss	546.3369965266111
C-GAN using ANN 5 Layer G & D BCELoss - EPS = 250	521.93539113172594
C-GAN using ANN 5 Layer G with Batch Norm of 3 Layers BCEwithLogitLoss	534.0923662798457
C-GAN using ANN 5 Layer G & D - BCELoss - Eps = 200 - z dim = 112	499.2763402028513

The BCEwithLogitLoss variant, while proficient, recorded a slightly higher FID score of 534.0923662798457.

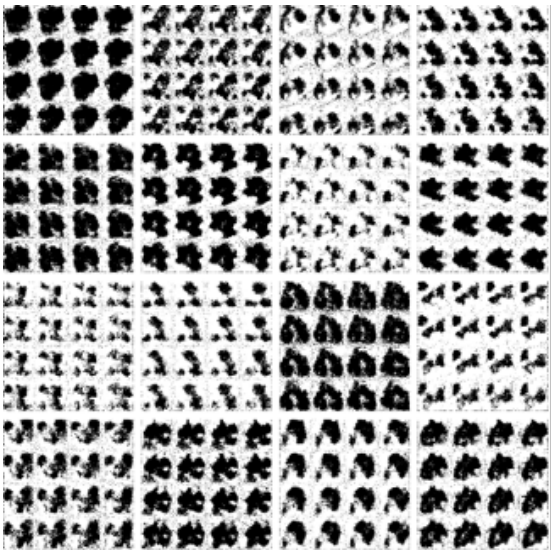

Fig. 11. Illustrates the C-GAN generated Image on 5-Layer with BCE Loss.

- **5 Layer C-GAN Architecture with MSE LOSS:**

Building upon the 5 Layer BCE architecture, our next phase involved transitioning to Mean Squared Error (MSE) loss while incorporating batch normalisation within the network. This strategic shift led to five distinct combinations under the 5-layer C-GAN architecture. The integration of batch normalisation significantly enhanced the model's performance, marking a notable improvement in this series. During our evaluation, the FID scores (see Table IV) across the different MSE loss combinations were relatively close, indicating consistent performance across variations.

TABLE IV

LLUSTRATES THE FID SCORE FOR 5 LAYER C-GANS WITH MSE LOSS

C-GAN Combination Names	FID Score
C-GAN using ANN with 5 Layer G with BN of 2 Layers MSELoss	490.48425102849024
C-GAN using ANN with 5 Layer G with BN of 3 Layers MSELoss	491.16758050569006
C-GAN using ANN with 5 Layer G with No BN Layers MSELoss	531.6123213796026
C-GAN using ANN with 5 Layer G with BN of 1 Layers MSELoss Tuning	491.2249674784682
C-GAN using ANN with 5 Layer G with Batch Norm of 1 Layers MSELoss	488.8694451641635

The standout combination in this series was the C-GAN model with a 5-layer generator and discriminator, supplemented by a single batch normalisation layer, which achieved the best FID score of 488.8694451641635 and the generated images are shown in Figure 12.

- **6 Layer C-GAN Architecture:**

Exploring further into the Conditional Generative Adversarial Networks, we advanced to a 6-layer C-GAN architecture, focusing exclusively on Binary Cross-Entropy (BCE) loss due to its previously demonstrated efficacy. In this study segment, we

executed three unique combinations within this architecture and the FID scores are shown in Table V below.

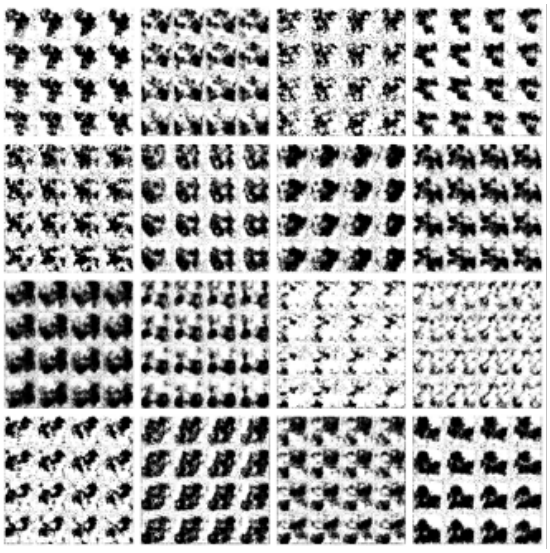

Fig. 12. Illustrates the C-GAN generated Image on 5-Layer with MSE Loss.

TABLE V

ILLUSTRATES THE FID SCORE FOR 6 LAYER C-GANS ARCHITECTURE.

C-GAN Combination Names	FID Score
C-GAN using ANN 6 Layer G & D - BCELoss - Eps = 200 - z dim = 112	494.44503296931066
C-GAN using ANN 6 Layer G & D - BCELoss - Eps = 200 - z dim = 112 Tuning	492.40832407514593
C-GAN using ANN 6 Layer G & D layer D - BCELoss - Eps = 200 - z dim = 112	481.208204647738286

The standout model was a C-GAN with a 6 Layer Generator and a 5 Layer Discriminator, which achieved an FID score of 481.0208467738286, as shown in Figure 13.

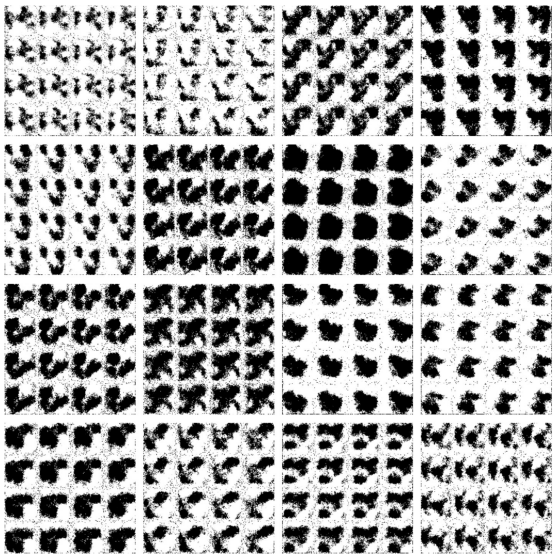

Fig. 13. Illustrates the C-GAN generated Image on 6-Layer Architecture.

The other two combinations also showcased commendable performances, with only a marginal FID score deviation of approximately 10 points. Visual inspections of the generated topographies further affirmed the quality of these models, reinforcing the 6-Layer C-GAN architecture's efficacy in creating detailed and realistic synthetic images.

- **7- and 8-Layer C-GAN Architectures:**

Our exploration of the 7 and 8 Layer Conditional Generative Adversarial Networks (C-GANs) architectures resulted in the development of 10 varied combinations, each showing promising results shown in Table VI.

These advanced layers significantly impacted the model's performance, as evidenced by their Frechet Inception Distance´ (FID) scores. The standout combination in the 7 Layer CGAN architecture, utilizing a z-dimension of 112 and running for 250 epochs, achieved an impressive FID score of 473.150113626764, as shown in Figure 14.

TABLE VI

ILLUSTRATES THE FID SCORE FOR 7- AND 8-LAYER C-GANS ARCHITECTURE.

C-GAN Combination Names	FID Score
C-GAN using ANN 7 - Layer G & D - BCELoss - Eps = 250 - z dim = 112 - COMBO-2	493.317999884040844
C-GAN using ANN 7 - Layer G & D - BCELoss - Eps = 250 - z dim = 112 COMBO-1 Tuning	516.1787562910203
C-GAN using ANN 7 - Layer G & D - BCELoss - Eps = 250 - z dim = 112 COMBO-1	473.1501136267864
C-GAN using ANN 7 - Layer G & D - layer D - BCELoss - Eps = 250 - z dim = 112	502.9392878074866
C-GAN using ANN 8 - Layer G & D BCELoss Eps = 250 - z dim = 112 COMBO-2 Tuning	490.2710705368761
C-GAN using ANN 8 - Layer G & D BCELoss Eps = 250 - z dim = 112 COMBO-2	480.23182042292456
C-GAN using ANN 8 - Layer G & D BCELoss Eps = 250 - z dim = 112 COMBO-1 Tuning	516.9473424725257
C-GAN using ANN 8 - Layer G & D - BCELoss - Eps = 250 - z dim = 112 - COMBO-3	486.6516508494069
C-GAN using ANN 8 - Layer G & D - BCELoss - Eps = 250 - z dim = 112 - COMBO-3	511.3109082678178
C-GAN using ANN 8 - Layer G & D - BCELoss - Eps = 250 - z dim = 112 - COMBO-2-1	484.1471982282307

Similarly, in the 8-layer architecture, a combination with the same z-dimension and epoch count reached an FID score of 480.23128042229456. Visually, the generated topographies across these configurations were impressive. This phase of our research highlighted the benefits of deeper layers in C-GANs for generating intricate biomaterial topographies and provided valuable insights for future model enhancements.

In our comprehensive evaluation of Conditional Generative Adversarial Networks (C-GANs), we analysed the performance of various architectures, loss functions, and other critical factors through Fréchet Inception Distance (FID) scores. Our results revealed a noteworthy performance of the 4-layer C-GAN architecture utilizing Binary Cross Entropy (BCE) loss, which surpassed its 5-layer counterpart operating under the same loss function. However, a significant advancement was observed when the 5 Layer architecture incorporated Mean Squared Error (MSE) Loss with Batch Normalization. Although it secured the second-best position, this combination showcased the potential impact of strategic choices in layers and loss functions, opening new avenues for model optimization.

As the research advanced, it became apparent while

Fig. 14. Illustrates the C-GAN generated Image on 7-Layer Architecture.

MSE Loss initially showed promise, BCE Loss consistently delivered more promising results. This was particularly evident when comparing the 6-layer C-GAN architecture, which predominantly utilized BCE Loss, to the 5-layer setup with MSE Loss. The 6-layer model demonstrated superior performance, underscoring the effectiveness of BCE Loss in our context.

Remarkably, the 7-Layer C-GAN architecture, configured with a z-dimension of 112 and extended to 250 epochs, emerged as the most successful model than the 4-layer CGAN architecture. This setup achieved better FID scores than all other configurations, including the 8-layer architecture. Despite the close competition among four-layer C-GAN and 7 Layer C-GAN combinations, the 7 Layer C-GAN model distinctively stood out, proving the most effective in our entire research for generating conditional topographies.

The 7-layer C-GAN architecture, finely tuned with a z-dimension of 112 and extended over 250 epochs, outperformed the 4-layer model. It achieved the best FID scores across all configurations, including the 8 Layer variants. The latter stood out in the tightly contested race between the 4-layer and 7layer C-GAN models. The 4 Layer model, while marginally outperformed, still showcased remarkable capabilities in generating topographies with less complexity considered best performing among all. It proved the most effective approach in our research for developing conditional topographies, affirming its pivotal role in advancing biomaterial topography synthesis.

C. Deep Convolutional Generative Adversarial Network

Our exploration of Deep Convolutional Generative Adversarial Networks (DC-GANs) in biomaterial topography synthesis involved diverse experiments, focusing on different topography patterns and data pre-processing techniques. This section presents the evaluation results for DC-GANs, particularly emphasizing their performance in generating one-by-four and four-by-four topographies and their effectiveness in handling gradient filter-applied topographies.

The one-by-four topography experiments were conducted using the standard dataset of 2176 images, aiming to test the model's actual performance on a common dataset. In contrast, the four-by-four topography experiments utilized resized and rotated datasets because it is evident that increased sample size improves the performance of the Gans. Additionally, we experimented with gradient-applied topographic datasets in one by four variants. The table below summarizes the FID scores for the various DC-GAN configurations (see Table VI) across these different topographies and datasets, highlighting the model's performance in each scenario.

TABLE VII

ILLUSTRATES THE FID SCORE FOR DC-GANS ARCHITECTURE.

DC-GAN Combination Names	FID Scores
1by4 - 128x128 Image Resolution - Residual Block - lr = 3	306.99759392703925
1by4 - Residual Block - Filters = 128 - EPs = 25	366.7584454440343384
1by4 - Residual Block - 128x128 Image Resolution - lr = 2	368.8870606060596
1by4 - Residual Block - Image Resolution 64X64 - 2	332.74408408683325
1by4 - Residual Block - Image Resolution 128X128 - Combo - 1	314.0494195522597
4by4 - Image Resolution - 128X128 - method - 1	423.28431532458493
4by4 - Image Resolution - 64X64	448.690626501754784
4by4 - Image Resolution - 256X256	325.47247543368325
1by4 - EDGE Processed Topography - Kernel Degree = 6 - 64 X 64 - EPS = 25	273.1905145542704
1by4 - EDGE Processed Topography - Kernel Degree = 8 - 64 X 64 - EPS = 25	276.3324416618382

In the initial phase, the research focused on a one-by-four topography to test the efficacy of DC-GANs in synthesizing biomaterial topographies. Out of a dozen configurations trialed, nine were subjected to a thorough evaluation, and from these, six were selected for in-depth analysis based on their superior performance. Remarkably, the DC-GAN tailored for one-by-four topography, which was configured with a resolution of 128x128 and augmented with residual blocks and an optimized learning rate of 0.0002, emerged as the top performer, which achieved an impressive FID score of 306.99795392703925 as shown in Figure 15.

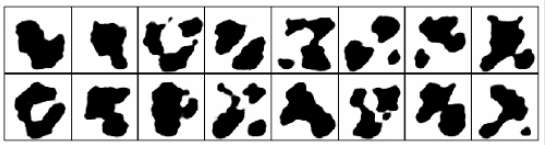

Fig. 15. Illustrates the DC-GAN generated Image on one-by-four topography.

During the second phase of our DC-GAN evaluation, we shifted our focus to edge-processed topographies. This advanced phase examined the model's ability to handle more intricately processed data. We conducted experiments on one by four topographies that were processed using an edge detection kernel. Among the configurations tested, the one employing a kernel degree 6 for edge processing stood out.

With an image resolution of 64x64, this configuration achieved a notable FID score of 273.1905145542704 and the generated image is shown in Figure 16.

Fig. 16. Illustrates the DC-GAN generated Image on one-by-four EDGE topography Dataset.

The third phase of our DC-GAN exploration delved into generating four-by-four topographies, leveraging an expanded sample size to challenge the model's capabilities further. Among the three combinations tested, the DC-GAN with a 256x256 image resolution and residual blocks showcased a commendable FID score of 325.47247543368235 as shown in Figure 17.

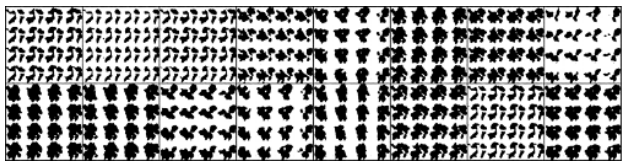

Fig. 17. Illustrates the DC-GAN generated Image on four-by-four topography.

This score suggested a significant achievement of the DCGAN in closely matching the distribution of the generated images to that of the original dataset. However, upon close visual inspection, certain limitations of the DC-GAN variants surfaced. These included inconsistencies in maintaining the repetitive structure across the topographical images and other aspects, suggesting areas for future refinement in the model's architecture and training regimen.

Notably, the model needed help with the repetitive structure within the topographies. The generated images revealed a dichotomy, with half reflecting uniformity in pattern repetition, while some objects suggested a potential need for additional epochs in training. Moreover, a tendency towards mode collapse was observed, as evidenced by the generation of non-distinct, repetitive samples, indicating challenges in the model's diversity and uniqueness in sample generation.

We observed some noteworthy results in our DC-GAN evaluations, particularly with the four-by-four topographies. Apart from the model with a 256x256 resolution, which achieved an FID score of 325.47247543368235, another significant configuration was "4by4 - Image Resolution - 128X128 method - 1," scoring an FID of 423.28431534258493 as shown in Figure 18.

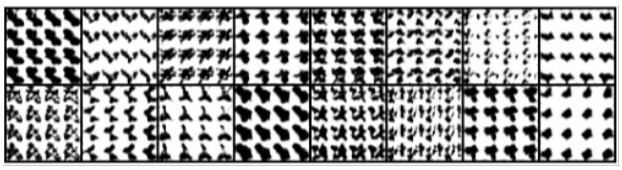

Fig. 18. Illustrates the DC-GAN generated Image on four-by-four topography of resolution 128X128.

While this model demonstrated a commendable level of detail and distribution accuracy, it exhibited similar issues as other DC-GAN configurations. These included challenges in maintaining repetitive structures and a tendency towards mode collapse. This reinforces the conclusion that, despite some successes in image resolution and training stability, the DC-GAN models still require further refinement to address these recurring issues in synthetic image generation fully. This analysis underscores their strengths in generating high fidelity biomaterial topographies and identifies future model enhancements and training optimization opportunities.

D. Wasserstein Generative Adversarial Network

Our pursuit of generating accurate biomaterial topographies led us to Wasserstein GANs (WGANs), which promise enhanced training stability and better convergence behaviour. The evaluation of WGANs focused on two primary patterns of topographies: one by four and four by four and the FID scores are shown in Table VIII.

TABLE VIII

ILLUSTRATES THE FID SCORE FOR W-GANS ARCHITECTURE.

W-GAN Combination Names	FID Scores
1 by 4 - topo - Image Resolution 64 X 64 - lr = 3 - z dim = 112 - EPS = 40	308.46295284878675
1 by 4 topo - Image Resolution 64 X 64 - lr = 3 - z dim = 112	316.8177227020753
1 by 4 topo - Image Resolution 64 X 64 - lr = 2 - z dim = 112 - EPS = 40	306.24041750456994
1 by 4 topo - Image Resolution 64X64 - lr = 3 - z dim = 112 - EPS = 40 - Filters = 128	336.02767974263675
1 by 4 topo - Image Resolution 64 X 64 - lr = 3 - z dim = 100	322.11463194263371
1 by 4 topo - Image Resolution 64X64 - lr = 3 - z dim = 112 - EPS = 40 - Filters = 96	353.68060268620761
4 by 4 - Image Resolution 64 X 64 - lr = 3 - EPS = 30	422.73968429157624
4 by 4 - Image Resolution 64X64 - lr = 3 - EPS = 40 - Filter = 128	407.62409949460357
4 by 4 - Image Resolution 64X64 - lr = 3 - EPS = 40	427.86826924886811
4 by 4 - Image Resolution 64 X 64 - lr = 2	419.3718606046734

For the one-by-four topography, we observed a notable improvement in performance and stability compared to previous models. The WGANs consistently generated topographies with high fidelity and fewer repetitions, suggesting a more robust learning of the underlying data distribution. Among the configurations tested, the model with an image resolution of 64x64, a learning rate of 2, and a z-dimension of 112 for 40 epochs stood out with an FID score of 306.24041750465994, indicating a high resemblance to the real data distribution as shown in Figure 19.

In the four-by-four topography experiments, WGANs demonstrated improved stability, yet some challenges reminiscent of those encountered with DC-GANs persisted. Despite the improvements, WGANs were still subject to certain

limitations, including an incomplete replication of the topographical patterns and a tendency towards non-uniformity in the generated images. The best-performing model in this category, featuring an image resolution of 64x64, a learning rate of 3, and a filter size of 128, achieved an FID score of 407.6240499460357, as shown in Figure 20.

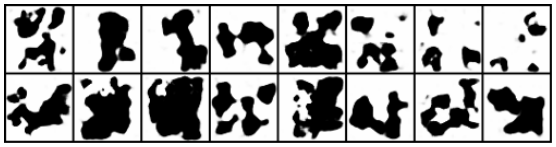

Fig. 19. Illustrates the W-GAN generated Image on one-by-four topography.

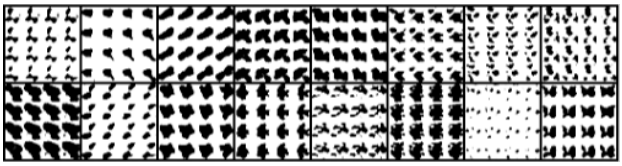

Fig. 20. Illustrates the W-GAN generated Image on four-by-four topography.

The best-performing model in this category, featuring an image resolution of 64x64, a learning rate of 3, and a filter size of 128, achieved an FID score of 407.6240499460357, as shown in Figure 20.

These results underscore the advancements made with WGANs in our quest for high-fidelity synthetic topographies. The reduced issues relative to DC-GANs and the WGANs' inherent training stability provide a strong foundation for future research to build upon. The insights gathered from this research phase will be instrumental in guiding the next steps toward creating even more accurate and stable models for biomaterial topography generation.

E. Comparative Analysis of GAN Variants

As our research progressed through the exploration of various Generative Adversarial Network (GAN) architectures, we systematically analysed and performed a comparative analysis of the combinations and results of each GAN variable in synthesizing biomaterial topographies.

In the context of one-by-four topographies, Vanilla GANs initially showed promising results. However, as we transitioned to Deep Convolutional Generative Adversarial Networks (DCGANs), the benefits of their unique integration of residual blocks and proficiency in handling 128X128 image resolutions became apparent, leading to a noticeable improvement over Vanilla GANs. Advancing further, Wasserstein GANs (WGANs) exhibited even greater proficiency in handling one by four topographies. Despite the Fréchet Inception Distance´ (FID) scores showing only slight differences between the best DC-GAN and WGAN models, WGANs excelled in generating high-quality images at a reduced resolution compared to DCGANs and, importantly, in producing a wider variety of unique samples.

In the case of four-by-four topographies, while Vanilla GANs exhibited solid performance, Conditional GANs (CGANs) marked a significant step forward. Although convolutional variants like DC-GANs and WGANs outperformed other models in terms of overall handling, they fell short in maintaining the repetitive structural integrity of the topographies, a fundamental aspect of our research goal. Moreover, a recurring issue became apparent upon monitoring the training loops via the tensor board: the DC-GAN models would begin to converge on an image only to regress and start the generation process anew, as if from scratch. This behaviour suggested a need for more stability in the training process, which significantly impedes achieving consistent results. While the WGANs did not entirely overcome the issues identified in DCGANs, they significantly reduced these problems, underscoring their potential in biomaterial topography synthesis. The diminished issues from DC-GANs indicate a move in the right direction yet also highlight the need for further refinement in model architecture and training strategies.

Our innovative approach, tailored for one-by-four and four-by-four topographies, superseded all other variants in closely mirroring the probability distribution of the real images. Notably, the DC-GAN model, tailored explicitly for gradient applied one-by-four topographic datasets, emerged as the standout performer in its category. Meanwhile, Vanilla GANs demonstrated the most effective performance in the four-by-four topography domain, particularly those with an increased sample size. This journey through various GAN architectures illuminated the strengths and limitations of each variant and significantly contributed to our understanding of practical techniques for biomaterial topography synthesis.

VI. DISCUSSION

This research embarked on a journey to explore the efficacy of various Generative Adversarial Network (GAN) models in synthesizing biomaterial topographies, directly addressing the burgeoning need for advanced computational methods in biomaterial discovery. Our comprehensive experimentation across various GAN models has unequivocally demonstrated that generative AI, particularly GANs, is proficient in creating topographical images. The successful generation of four-by-four detailed topographies is a testament to the capability of GANs to accurately capture spatial hierarchies and replicate the repetitive structural patterns inherent in these complex topographies.

In our study, the application of Conditional Generative Adversarial Networks (C-GANs) has successfully demonstrated their ability to generate images that closely align with specific

labels, such as attachment levels in topographies. This finding validates the feasibility of using GANs to create topographies based on predetermined criteria like attachment levels. The favourable Fréchet Inception Distance (FID) scores obtained´ from our experiments provide strong evidence that the distribution of the generated images closely resembles that of the real data. This result indicates the GANs' capability to produce high-quality synthetic topographic photos that are virtually indistinguishable from their original counterparts, thus reinforcing the potential of GANs in precise and conditioned image generation.

In our innovative approach to this research, we meticulously explored the capabilities of Generative Adversarial Networks (GANs) in biomaterial topography synthesis, addressing key aspects. Our results affirmatively demonstrated that the two two-by-two cropped topographies could effectively retain essential spatial information between structures. This capability is pivotal in advancing the study of biomaterial discovery, as it underscores the potential of GANs to produce high-quality images while potentially reducing computational demands. By adeptly handling varied input dimensions, our approach suggests a pathway to enhance the efficiency and effectiveness of GAN models in this field. Further, we scrutinized the GANs' proficiency in focusing on topography shapes, particularly when processing images specifically pre-processed (gradient-applied topographies) to highlight distinct features. Our models showcased an impressive ability by handling the one-by-four gradient applied topographies, achieving a close match to the real image distribution, and delivering superior performance compared to other models.

Furthermore, we assessed the impact of augmenting the sample size of topographies through rotation techniques. Our findings conclusively revealed that increasing the dataset size enhances the model's performance, providing new insights into the dynamics of generative modelling. In cases with limited data samples, we observed that Multilayer Perceptron (MLP) architectures generally surpass Convolutional Neural Network (CNN) based models in performance. These finding highlights MLPs' effectiveness in smaller datasets. Moreover, we noted a clear trend in increased sample size consistently improved model efficiency, particularly with MLP architectures. CNN based architectures subsequently require more samples than MLP models.

This research journey led us to a vital conclusion regarding the distinct strengths of Multilayer Perceptron (MLP) and Convolutional Neural Network (CNN) architectures in biomaterial topography synthesis. We discovered that MLP architectures excel in feature mapping, capturing crucial topographical information. Conversely, CNN architectures excel in summarizing information, which makes them less suitable for intricate tasks such as handling four-by-four or two-by-two topographies. This differentiation was evident when MLP based GANs struggled with gradient-applied topographies, a domain where CNNs typically thrive.

Our study also ventured into a hybrid approach, integrating three ANN layers for initial mapping followed by convolutional layers, particularly for four-by-four datasets. Despite the innovative concept, this approach did not produce the anticipated results, offering valuable lessons instead.

VII. LIMITATIONS

In concluding our comprehensive exploration of Generative Adversarial Networks (GANs) for biomaterial topography synthesis, it is crucial to acknowledge the limitations encountered in this research. We gained invaluable insights throughout the study, from training GANs with limited sample sizes to overcoming issues related to vanishing gradients and training stability.

- **Dataset Size and Diversity:** Our study highlighted the dependency of GANs on extensive, varied datasets. Increasing sample sizes through techniques like image rotation improved performance; however, the reliance on large datasets can be challenging in scenarios with limited data availability. Especially in conditioned topography generation, the inability to expand the dataset size with varied conditions was a notable constraint.
- **Model Complexity:** While advanced models like DCGANs and WGANs excelled in generating detailed topographies, they sometimes needed help with uniformity and avoiding repetitive patterns, particularly in 4 by4 topographies. This underscores the need for further model refinement to handle more complex structures with greater diversity.
- **Computational Constraints:** A significant challenge was the computational expense of advanced GAN models. The high resource demands of DC-GANs and WGANs, established by numerous studies, necessitate considerable computational power, which imposes significant constraints on our research and can be a limiting factor in contexts with restricted computational capabilities.

These limitations, while highlighting the challenges faced, also shed light on potential areas of improvement and exploration. They underscore the need for ongoing innovation in GAN research, particularly in optimizing models for diverse and limited datasets and in developing more computationally efficient architectures.

VIII. CONCLUSION

This study was aimed at exploring the application of Generative Adversarial Networks (GANs) in the discovery of biomaterial topographies, assessing the capacity of GANs to generate such structures and identifying potential obstacles in

the process. Our findings reveal that GANs indeed have the capability to produce topographies closely aligned with training data, uncovering crucial insights that could pave the way for AI-driven biomaterial discovery. However, our research also highlighted significant challenges inherent to using GANs.

A recurrent issue encountered during the GAN training process was model collapse. Even with advanced GAN variants, we could only minimize rather than fully eliminate this problem. Training instability was another challenge, albeit mitigated to an extent sufficient for image generation. Employing convolutional architectures in GANs often led to non-convergence, which we addressed with unique techniques to reduce its frequency. Interestingly, increasing the pixel size of input images enhanced the quality and accuracy of the generated topographies, moving them closer to the real image's probability distribution. However, this approach often triggered the vanishing gradient problem, which we were able to overcome with innovative methods.

The computational demands of GANs posed further difficulties, particularly when exploring high-resolution topographies, leading to extended training durations. We noticed that after a certain level of training, the models began to produce less diverse samples and showed tendencies of overfitting. Another challenge was the reconstruction of images during generation, yet the learning ability of GANs proved advantageous, managed the models to capture patterns and generate topographies effectively.

Despite these challenges, our research yielded comprehensive findings and an enhanced understanding of the dataset lead us to affirm that Generative Adversarial Networks (GANs) can be effectively integrated with other technologies to optimize the generation of topographies, offering the potential for promising results. Our innovative approaches have been well-aligned with the capabilities of the model, demonstrating the feasibility of using our insights to expedite the process of achieving significant outcomes. Nevertheless, our findings emphasize the crucial role of architecture selection in GANs, opening possibilities for exploring diverse models and architectures for future biomaterial research, as elaborated in the next section.

IX. FUTURE RECOMMENDATIONS

Considering our comprehensive exploration of Generative Adversarial Networks (GANs) for biomaterial topography synthesis, this research has yielded significant insights and uncovered areas ripe for further investigation. While we have successfully demonstrated the potential of various GAN models in generating detailed topographies, we propose innovative approaches based on our findings as the following future recommendations:

- **Utilization of Auxiliary GANs:**
  To enhance the generation of conditioned topographies, we recommend the exploration of Auxiliary GANs [72]. In Auxiliary GANs, the discriminator not only differentiates between real and fake data but also performs classification. This dual task compels the generator to produce data that is both realistic and accurately classified as per the auxiliary task. This advanced GAN architecture could offer more nuanced control and better-quality generation in conditioned environments.
- **Evaluating Conditional GANs with a Classification Model:**
  Building a classification model using existing datasets, such as the 2100 images with attachment levels, could provide a novel approach to evaluate the efficacy of CGANs and other GAN-generated images. This method could be an innovative benchmarking tool for assessing the accuracy of generated images against specific conditions.
- **Experimentation with Auto Encoders and Their Variants:**
  Given the challenges faced in feature mapping, image reconstruction and diversity in the samples, future research could benefit from incorporating Auto Encoders [73], including Variational Auto Encoders [74] and Adversarial Auto Encoders [75] and their conditional variants [76]. These models are renowned for their prowess in feature extraction and reconstruction [78], and they could complement GANs in generating more accurate and diverse biomaterial topographies.
- **Hybrid Model Implementation:** We suggest employing hybrid models that combine the strengths of GANs and Auto Encoders variants, such as VAE-GANs and AAEGANs [77]. Based on our insights, this integrative approach would enhance performance in generating biomaterial topographies, potentially overcoming limitations observed in standalone GAN models.
- **Focus on Gradient-Applied Topography Dataset:** Our research has shown that the gradient-applied topography dataset yielded the most promising results. Therefore, we recommend prioritizing this dataset in future studies, as it demonstrated a high degree of alignment with the distribution of real images, indicating its potential for yielding highly accurate synthetic topographies.
- **Focus on two-by-two and Augmented Dataset:** Future research should also delve into the potential of two-by-two and augmented datasets. Our findings indicate that enlarging the pixel size of images enhances model performance. Hence, employing two-by-two topographies could be an effective strategy for increasing pixel size while reducing computational resources for efficiency. Alongside this, we would encourage the utilization of the resized and rotated dataset as these

techniques have been shown to significantly enhance model performance, offering a promising direction for future research.

These recommendations aim to build on the successes and learnings of our current research, paving the way for more refined and effective generative models in the field of biomaterial synthesis.

REFERENCE

[1] Wilson, Natalia & Reich, Amanda & Graham, Jove & Bhatt, Deepak & Nguyen, Louis & Weissman, Joel. (2021). Patient perspectives on the need for implanted device information: Implications for a post-procedural communication framework. Health Expectations. 24. 10.1111/hex.13273.

[2] Jiang G, Zhou DD. Technology advances and challenges in hermetic packaging for implantable medical devices. In: Zhou DD, Greenbaum ES, editors. *Implantable neural prostheses 2: techniques and engineering approaches.* Berlin: Springer; 2010. pp. 28–61.

[3] Vassey, Matthew & Ma, Le & Kämmerling, Lisa & Mbadugha, Chidimma & Trindade, Gustavo & Figueredo, Grazziela & Pappalardo, Francesco & Hutchinson, Jason & Markus, Robert & Rajani, Seema & Hu, Qin & Winkler, David & Irvine, Derek & Hague, Richard & Ghaemmaghami, Amir & Wildman, Ricky & Alexander, Morgan. (2023). Innate immune cell instruction using micron-scale 3D objects of varied architecture and polymer chemistry: The ChemoArchiChip. Matter. 6. 10.1016/j.matt.2023.01.002.

[4] Abu-Amer, Y., Darwech, I., and Clohisy, J.C. (2007). Aseptic loosening of total joint replacements: mechanisms underlying osteolysis and potential therapies. Arthritis Res. Ther. 9, S6. https://doi.org/10.1186/ar2170. [5] Jain, N., and Vogel, V. (2018). Spatial confinement downsizes the inflammatory response of macrophages. Nat. Mater. 17, 1134–1144. https://doi.org/10.1038/s41563- 018-0190-6. [6] McWhorter, F.Y., Wang, T., Nguyen, P., Chung, T., and Liu, W.F. (2013). Modulation of macrophage phenotype by cell shape. Proc. Natl. Acad. Sci. USA 110, 17253–17258. https:// doi.org/10.1073/pnas.1308887110.

[7] Milton, J.M. (1992). Poly(Ethylene Glycol) Chemistry: Biotechnical and Biomedical Applications (Springer US). https://doi.org/10. 1007/978-1-4899-0703-5.

[8] Hucknall, A., Rangarajan, S., and Chilkoti, A. (2009). In pursuit of zero: polymer brushes that resist the adsorption of proteins. Adv. Mater. 21, 2441–2446. https://doi.org/10.1002/adma. 200900383.

[9] Chapman, D. (1993). Biomembranes and new hemocompatible materials. Langmuir 9, 39–45. https://doi.org/10.1021/la00025a012.

[10] Liu, Q., Chiu, A., Wang, L.-H., An, D., Zhong, M., Smink, A.M., de Haan, B.J., de Vos, P., Keane, K., Vegge, A., et al. (2019). Zwitterionically modified alginates mitigate cellular overgrowth for cell encapsulation. Nat. Commun. 10, 5262. https://doi.org/10.1038/ s41467-019-13238-7.

[11] Vegas, A.J., Veiseh, O., Doloff, J.C., Ma, M., Tam, H.H., Bratlie, K., Li, J., Bader, A.R., Langan, E., Olejnik, K., et al. (2016). Combinatorial hydrogel library enables identification of materials that mitigate the foreign body response in primates. Nat. Biotechnol. 34, 345–352. https://doi.org/10.1038/nbt.3462.

[12] Vegas, A.J., Veiseh, O., Gu¨rtler, M., Millman, J.R., Pagliuca, F.W., Bader, A.R., Doloff, J.C., Li, J., Chen, M., Olejnik, K., et al. (2016). Long-term glycemic control using polymer-encapsulated human stem cell-derived beta cells in immune- competent mice. Nat. Med. 22, 306–311. https://doi.org/10.1038/nm.4030.

[13] Chen, S., Jones, J.A., Xu, Y., Low, H.Y., Anderson, J.M., and Leong, K.W. (2010). Characterization of topographical effects on macrophage behavior in a foreign body response model. Biomaterials 31, 3479–3491. https://doi.org/10.1016/j.biomaterials.2010. 01.074. [14] Luu, T.U., Gott, S.C., Woo, B.W.K., Rao, M.P., and Liu, W.F. (2015). Micro- and nanopatterned topographical cues for regulating macrophage cell shape and phenotype. ACS Appl. Mater. Interfaces 7, 28665–28672. https://doi.org/10.1021/acsami.5b10589.

[15] A. Osokin, A. Chessel, R. E. C. Salas and F. Vaggi, "GANs for Biological Image Synthesis," 2017 IEEE International Conference on Computer Vision (ICCV), Venice, Italy, 2017, pp. 2252-2261, doi: 10.1109/ICCV.2017.245.

[16] Blanchard, Andrew & Stanley, Christopher & Bhowmik, Debsindhu. (2021). Using GANs with adaptive training data to search for new molecules. Journal of Cheminformatics. 13. 10.1186/s13321-021-00494-3.

[17] *Baniukiewicz P, Lutton EJ, Collier S and Bretschneider T (2019) Generative Adversarial Networks for Augmenting Training Data of Microscopic Cell Images. Front. Comput. Sci. 1:10. doi: 10.3389/fcomp.2019.00010*

[18] Menon, Dhruv & Ranganathan, Raghavan. (2022). A Generative Approach to Materials Discovery, Design, and Optimization. ACS Omega. 7. 10.1021/acsomega.2c03264.

[19] Y. Zhang, D. Zhao, J. Zhang, R. Xiong and W. Gao, "Interpolation-Dependent Image Downsampling," in *IEEE Transactions on Image Processing*, vol. 20, no. 11, pp. 3291-3296, Nov. 2011, doi: 10.1109/TIP.2011.2158226.

[20] Rivest, Francois & Soille, Pierre & Beucher, Serge. (1993). Morphological gradients. J. Electronic Imaging. 2. 326-336. 10.1117/12.159642.

[21] Huang G, Jafari AH. Enhanced balancing GAN: minority-class image generation. Neural Comput Appl. 2023;35(7):5145-5154. doi: 10.1007/s00521-021-06163-8. Epub 2021 Jun 17. PMID: 34177125; PMCID: PMC8211314.

[22] Hu, Mengxiao & Li, Jinlong. (2019). Exploring Bias in GAN-based Data Augmentation for Small Samples. https://doi.org/10.48550/arXiv.1905.08495

[23] D. Lee, S. Lee, H. Lee, K. Lee and H. -J. Lee, "Resolution-Preserving Generative Adversarial Networks for Image Enhancement," in IEEE Access, vol. 7, pp. 110344-110357, 2019, doi: 10.1109/ACCESS.2019.2934320.

[24] Lim, Bee & Son, Sanghyun & Kim, Heewon & Nah, Seungjun & Lee, Kyoung Mu. (2017). Enhanced Deep Residual Networks for Single Image Super-Resolution. 1132-1140. 10.1109/CVPRW.2017.151.

[25] Lai, Wei-Sheng & Huang, Jia-Bin & Ahuja, Narendra & Yang, Ming-Hsuan. (2017). Fast and Accurate Image Super-Resolution with Deep Laplacian Pyramid Networks. IEEE Transactions on Pattern Analysis and Machine Intelligence. PP. 10.1109/TPAMI.2018.2865304.

[26] Z. Wang, J. Chen and S. C. H. Hoi, "Deep Learning for Image Super-Resolution: A Survey," in IEEE Transactions on Pattern Analysis and Machine Intelligence, vol. 43, no. 10, pp. 3365-3387, 1 Oct. 2021, doi: 10.1109/TPAMI.2020.2982166.

[27] Rukundo, O., & Cao, H. (2012). Nearest Neighbor Value Interpolation. *ArXiv, abs/1211.1768*.

[28] K. T. Gribbon and D. G. Bailey, "A novel approach to real-time bilinear interpolation," Proceedings. DELTA 2004. Second IEEE International Workshop on Electronic Design, Test and Applications, Perth, WA, Australia, 2004, pp. 126-131, doi: 10.1109/DELTA.2004.10055.

[29] Fardo, Fernando & Conforto, Victor & Oliveira, Francisco & Rodrigues, Paulo. (2016). A Formal Evaluation of PSNR as Quality Measurement Parameter for Image Segmentation Algorithms.

[30] J. J. Danker Khoo, K. H. Lim and J. T. Sien Phang, "A Review on Deep Learning Super Resolution Techniques," 2020 IEEE 8th Conference on Systems, Process and Control (ICSPC), Melaka, Malaysia, 2020, pp. 134-139, doi: 10.1109/ICSPC50992.2020.9305806.

[31] Rehan, Ahmed & Akbar, Muhammad & Hanif, Muhammad & Shafique, Muhammad. (2023). SoC-GANs: Energy-Efficient Memory Management for System-on-Chip Generative Adversarial Networks. 10.1007/978-3-031-19568-6_9.

[32] K. He, X. Zhang, S. Ren and J. Sun, "Deep Residual Learning for Image Recognition," *2016 IEEE Conference on Computer Vision and Pattern Recognition (CVPR)*, Las Vegas, NV, USA, 2016, pp. 770-778, doi: 10.1109/CVPR.2016.90.

[33] C. Dong, C. C. Loy, K. He, and X. Tang. Learning a deep convolutional network for image super-resolution. In ECCV 2014. 2, 6, 7

[34] C. Ledig, L. Theis, F. Huszar, J. Caballero, A. Cunningham, A. Acosta, A. Aitken, A. Tejani, J. Totz, Z. Wang, et al. Photo-realistic single image super-resolution using a generative adversarial network. arXiv:1609.04802, 2016.

[35] Zaeemzadeh, Alireza et al. "Norm-Preservation: Why Residual Networks Can Become Extremely Deep?" *IEEE Transactions on Pattern Analysis and Machine Intelligence* 43 (2018): 3980-3990.

[36] Anwar, Saeed & Khan, Salman & Barnes, Nick. (2020). A Deep Journey into Super-resolution: A Survey. ACM Computing Surveys. 53. 1-34. 10.1145/3390462.

[37] C. Dong, C. C. Loy, and X. Tang. Accelerating the superresolution convolutional neural network. In ECCV 2016.

[38] - Joung, Yeun-Ho. (2013). Development of Implantable Medical Devices: From an Engineering Perspective. International neurourology journal. 17. 98-106. 10.5213/inj.2013.17.3.98.

[39] - W. Greatbatch and C. F. Holmes, "History of implantable devices," in *IEEE Engineering in Medicine and Biology Magazine*, vol. 10, no. 3, pp. 38-41, Sept. 1991, doi: 10.1109/51.84185.

[40] - Zoll, Paul M.. "Resuscitation of the heart in ventricular standstill by external electric stimulation." *The New England journal of medicine* 247 20 (1952): 768-71 .

[41] - Huebsch, N., Mooney, D. Inspiration and application in the evolution of biomaterials. *Nature* **462**, 426–432 (2009). https://doi.org/10.1038/nature08601

[42] - Lela Migirov, Elad Dagan & Jona Kronenberg (2009) Surgical and medical complications in different cochlear implant devices, Acta Oto-Laryngologica, 129:7, 741-744, DOI: 10.1080/00016480802398954

[43] - Jemt, Torsten. (2019). Implant failures and age at the time of surgery: A retrospective study on implant treatment in 2915 partially edentulous jaws. Clinical Implant Dentistry and Related Research. 21. 10.1111/cid.12812.

[44] - Davenport, T., & Kalakota, R. (2019). The potential for artificial intelligence in healthcare. *Future Healthcare Journal*, *6*(2), 94-98. https://doi.org/10.7861/futurehosp.6-2-94

[45] - Shokrollahi, Y., Yarmohammadtoosky, S., Nikahd, M. M., Dong, P., Li, X., & Gu, L. (2023). A Comprehensive Review of Generative AI in Healthcare. *ArXiv*. /abs/2310.00795

[46] - Ramesh, Aditya, Prafulla Dhariwal, Alex Nichol, Casey Chu, and Mark Chen. 2022. "Hierarchical TextConditional Image Generation with Clip Latents." arXiv Preprint arXiv:2204.06125

[47] - Morley J, DeVito NJ, Zhang J. Generative AI for medical research. BMJ. 2023 Jul 12;382:1551. doi: 10.1136/bmj.p1551. PMID: 37437947.

[48] - Arora, A., & Arora, A. (2022). Generative adversarial networks and synthetic patient data: Current challenges and future perspectives. *Future Healthcare Journal*, *9*(2), 190-193. https://doi.org/10.7861/fhj.2022-0013

[49] - Skandarani Y, Jodoin P-M, Lalande A. GANs for Medical Image Synthesis: An Empirical Study. *Journal of Imaging*. 2023; 9(3):69. https://doi.org/10.3390/jimaging9030069

[50] - Coto, Andrea & Precker, Christian & Andersson, Tom & Laukkanen, Anssi & Suhonen, Tomi & Rey Rodriguez, Pilar & Muiños-Landin, Santiago. (2023). The use of generative models to speed up the discovery of materials. Computer Methods in Material Science. 23. 10.7494/cmms.2023.1.0802.

[51] - Turing AM (2009) Computing Machinery and Intelligence. In: Epstein R, Roberts G, Beber G (eds) Parsing the Turing Test: Philosophical and Methodological Issues in the Quest for the Thinking Computer. Springer, Netherlands: Dordrecht, pp 23–65

[52] - Chollet F (2018) Deep learning with Python (Vol. 361). Manning, New York

[53] - Bian, Yuemin & Xie, Xiangqun. (2020). Generative chemistry: drug discovery with deep learning generative models.

[54] - Karhunen J, Raiko T, Cho KH. Unsupervised deep learning: a short review. In: Advances in independent component analysis and learning machines. 2015; p. 125–42.

[55] - Sarker, Iqbal. (2021). Deep Learning: A Comprehensive Overview on Techniques, Taxonomy, Applications and Research Directions. SN Computer Science. 2. 10.1007/s42979-021-00815-1.

[56] - Hinton GE, Osindero S, Teh Y-W. A fast learning algorithm for deep belief nets. Neural Comput. 2006;18(7):1527–54.

[57] - Jebara, Tony & Meila, Marina. (2006). Machine learning: Discriminative and generative. The Mathematical Intelligencer. 28. 67-69. 10.1007/BF02987011.

[58] - Goodfellow, I. J., Mirza, M., Xu, B., Ozair, S., Courville, A., & Bengio, Y. (2014). Generative Adversarial Networks. *ArXiv*. /abs/1406.2661

[59] - Zhang P, Kamel Boulos MN. Generative AI in Medicine and Healthcare: Promises, Opportunities and Challenges. *Future Internet*. 2023; 15(9):286. https://doi.org/10.3390/fi15090286

[60] - Dash, A., Ye, J., & Wang, G. (2021). A review of Generative Adversarial Networks (GANs) and its applications in a wide variety of disciplines -- From Medical to Remote Sensing. *ArXiv*. /abs/2110.01442

[61] - Yuan C, Deng K, Li C, Zhang X, Li Y. Improving Image Super-Resolution Based on Multiscale Generative Adversarial Networks. Entropy (Basel). 2022 Jul 26;24(8):1030. doi: 10.3390/e24081030. PMID: 35893009; PMCID: PMC9394415.

[61] - Akkaya, Berke & Çolakoğlu, Nurdan. (2019). Comparison of Multi-class Classification Algorithms on Early Diagnosis of Heart Diseases.

[62] - Srivastava, Nitish & Hinton, Geoffrey & Krizhevsky, Alex & Sutskever, Ilya & Salakhutdinov, Ruslan. (2014). Dropout: A Simple Way to Prevent Neural Networks from Overfitting. Journal of Machine Learning Research. 15. 1929-1958.

[63] - Li, Y., Ma, W., Chen, C., Zhang, M., Liu, Y., Ma, S., & Yang, Y. (2022). A Survey on Dropout Methods and Experimental Verification in Recommendation. *ArXiv*. /abs/2204.02027

[64] - Yazici, Yasin & Foo, Chuan-Sheng & Winkler, Stefan & Yap, Kim-Hui & Chandrasekhar, Vijay. (2020). Empirical Analysis Of Overfitting And Mode Drop In Gan Training. 1651-1655. 10.1109/ICIP40778.2020.9191083.

[65] - Mirza, M., & Osindero, S. (2014). Conditional Generative Adversarial Nets. *ArXiv*. /abs/1411.1784

[66] - Figueira, A., & Vaz, B. (2022). Survey on Synthetic Data Generation, Evaluation Methods and GANs. *Mathematics*, *10*(15), 2733. https://doi.org/10.3390/math10152733

[67] - Liu, Bingqi & Lv, Jiwei & Fan, Xinyue & Luo, Jie & Zou, Tianyi. (2022). Application of an Improved DCGAN for Image Generation. Mobile Information Systems. 2022. 10.1155/2022/9005552.

[68] - Radford, A., Metz, L., & Chintala, S. (2015). Unsupervised Representation Learning with Deep Convolutional Generative Adversarial Networks. *ArXiv*. /abs/1511.06434

[69] - Arjovsky, M., Chintala, S., & Bottou, L. (2017). Wasserstein GAN. *ArXiv*. /abs/1701.07875

[70] - Gulrajani, I., Ahmed, F., Arjovsky, M., Dumoulin, V., & Courville, A. (2017). Improved Training of Wasserstein GANs. *ArXiv*. /abs/1704.00028

[71] - Dash, A., Ye, J., & Wang, G. (2021). A review of Generative Adversarial Networks (GANs) and its applications in a wide variety of disciplines -- From Medical to Remote Sensing. *ArXiv*. /abs/2110.01442

[72] - Odena, A., Olah, C., & Shlens, J. (2016). Conditional Image Synthesis With Auxiliary Classifier GANs. *ArXiv*. /abs/1610.09585

[73] - Bank, D., Koenigstein, N., & Giryes, R. (2020). Autoencoders. *ArXiv*. /abs/2003.05991

[74] - Kingma, D. P., & Welling, M. (2019). An Introduction to Variational Autoencoders. *ArXiv*. https://doi.org/10.1561/2200000056

[75] - Makhzani, A., Shlens, J., Jaitly, N., Goodfellow, I., & Frey, B. (2015). Adversarial Autoencoders. *ArXiv*. /abs/1511.05644

[76] - Harvey, W., Naderiparizi, S., & Wood, F. (2021). Conditional Image Generation by Conditioning Variational Auto-Encoders. *ArXiv*. /abs/2102.12037

[77] - Yu, Fan & Xu, Mingyao & Chen, Shihui. (2022). VAE-GAN: Hybrid Generative Variational Autoencoder Generative.

[78] - Yuan, F.-N & Zhang, L. & Shi, J.-T & Xia, X. & Li, G.. (2019). Theories and Applications of Auto-Encoder Neural Networks: A Literature Survey. Jisuanji Xuebao/Chinese Journal of Computers. 42. 203-230. 10.11897/SP.J.1016.2019.00203.

[79] - Prakash, Nityanand & Kim, Jiseong & Jeon, Jieun & Kim, Siyeon & Arai, Yoshie & Bello, Alvin & Park, Hansoo & Lee, Soo-Hong. (2023). Progress and emerging techniques for biomaterial-based derivation of mesenchymal stem cells (MSCs) from pluripotent stem cells (PSCs). Biomaterials research. 27. 31. 10.1186/s40824-023-00371-0.

[80] - Hendrikse, Simone & Contreras-Montoya, Rafael & Ellis, Amanda & Thordarson, Pall & Steed, Jonathan. (2021). Biofunctionality with a twist: the importance of molecular organisation, handedness and configuration in synthetic biomaterial design. Chemical Society Reviews. 51. 10.1039/D1CS00896J.

[81] - Babani, K. (2023). The Journey of Biomaterial Discovery to Collaboration in Tissue Engineering And 3D Printing. *J Adv Biomed Eng*, 1(1), 3-7.

[82] - Pais AI, Belinha J, Alves JL. Advances in Computational Techniques for Bio-Inspired Cellular Materials in the Field of Biomechanics: Current Trends and Prospects. *Materials*. 2023; 16(11):3946. https://doi.org/10.3390/ma16113946

[83] - Mackay, Benita & Marshall, Karen & Grant-Jacob, James & Kanczler, Janos & Eason, Robert & Oreffo, Richard & Mills, Ben. (2021). The future of bone regeneration: Integrating AI into tissue engineering. Biomedical physics & engineering express. 7. 10.1088/2057-1976/ac154f.

[84] - Luu, Rachel & Buehler, Markus. (2023). BioinspiredLLM: Conversational Large Language Model for the Mechanics of Biological and Bio-Inspired Materials. Advanced Science. 10.1002/advs.202306724.

[85] - Chiang, Yu-Hsuan & Tseng, Bor-Yann & Wang, Jyun-Ping & Chen, Yu-Wen & Tung, Cheng Che & Yu, Chi-Hua & Chen, P.-Y & Chen, Chuin-Shan. (2023). Generating three-dimensional bioinspired microstructures using transformer-based generative adversarial network. Journal of Materials Research and Technology. 27. 10.1016/j.jmrt.2023.10.200.

[86] - Yang, L., Zhang, Z., Song, Y., Hong, S., Xu, R., Zhao, Y., Zhang, W., Cui, B., & Yang, M. (2022). Diffusion Models: A Comprehensive Survey of Methods and Applications. *ArXiv*. /abs/2209.00796

[87] - Croitoru, F., Hondru, V., Ionescu, R. T., & Shah, M. (2022). Diffusion Models in Vision: A Survey. *ArXiv*. https://doi.org/10.1109/TPAMI.2023.3261988

[88] - Afaq, S., & Rao, S. (2020). Significance Of Epochs On Training A Neural Network. *International Journal of Scientific & Technology Research, 9*, 485-488.

[89] - Hecht-Nielsen, "Theory of the backpropagation neural network," *International 1989 Joint Conference on Neural Networks*, Washington, DC, USA, 1989, pp. 593-605 vol.1, doi: 10.1109/IJCNN.1989.118638.

[90] - Wang, Qi & Ma, Yue & Zhao, Kun & Tian, Yingjie. (2022). A Comprehensive Survey of Loss Functions in Machine Learning. Annals of Data Science. 9. 10.1007/s40745-020-00253-

[91] - Heusel, M., Ramsauer, H., Unterthiner, T., Nessler, B., & Hochreiter, S. (2017). GANs Trained by a Two Time-Scale Update Rule Converge to a Local Nash Equilibrium. *ArXiv*. /abs/1706.08500